Journal of Applied Pharmaceutical Science Vol. 15(12), pp 046-059, December, 2025
Available online at http://www.japsonline.com
DOI: 10.7324/JAPS.2025.v15.i12.6
ISSN 2231-3354

Development and evaluation of a proniosomal gel for palm tocotrienol-rich fraction topical delivery

Tanya Tong-en Fong[1], Puxvadee Chaiku[2], Kar Lin Nyam[3], Chee Chin Chu[4]*

[1]School of Pharmacy, Faculty of Health and Medical Sciences, Taylor's University, Subang Jaya, Malaysia.
[2]School of Cosmetic Science, Mae Fah Luang University, Chiang Rai, Thailand.
[3]Faculty of Applied Sciences, UCSI University, Kuala Lumpur, Malaysia.
[4]School of Pharmacy, Faculty of Health and Medical Sciences, Taylor's University, Subang Jaya, Malaysia.

ARTICLE HISTORY

Received on: 11/04/2025
Accepted on: 30/09/2025
Available Online: 05/11/2025

Key words:
Tocotrienol-rich fraction, proniosomal gel, niosomes, D-limonene, squalene.

ABSTRACT

Tocotrienol-rich fraction (TRF) is a potent antioxidant capable of counteracting skin aging-related changes. However, TRF poses challenges for effective skin delivery. This study aimed to optimize the concentration of terpenes in a proniosomal gel (PNG) for TRF delivery and evaluate its physical properties, antioxidant activity, and topical release kinetics. The PNGs were prepared using the coacervation-phase separation technique. Various concentrations of D-limonene and squalene, as well as combinations of both, were tested to determine their effects on the formulation. The antioxidant activities of the sample were analyzed using 2,2-diphenyl-1-picrylhydrazyl radical scavenging assay and the *in vitro* release of TRF was studied through a Franz diffusion cell. All formulations displayed particle size ranging from 271.60 to 416.40 nm. The optimized PNG (M5), which is composed of 2.5% D-limonene and 2.5% squalene in the PNG, exhibited the highest entrapment efficiency (98.530% ± 0.048%) and antioxidant activity (2.951 ± 0.028 mg TE/g sample). A high flow point and shear-thinning flow characteristics were found by rheological characterization. Its predominant elastic nature in both amplitude and frequency sweeps demonstrated that the M5 rheological and stability characteristics were satisfactory. The release profile of M5 showed sustained and controlled TRF release by non-Fickian diffusion, while the control formulations showed an immediate release of TRF. The study successfully determined the optimal concentration of terpenes in the PNGs with the greatest physical and antioxidant properties while outperforming control samples for the TRF release.

INTRODUCTION

Palm tocotrienol-rich fraction

Aging-related changes in skin physiology, including diminished functionality and increased oxidative stress, enforce the need for effective antioxidant interventions [1,2]. Palm tocotrienol-rich fraction (TRF) represents a promising natural compound in cosmeceuticals, owing to its significant antioxidant and anti-inflammatory properties which make it an ideal candidate for anti-aging applications [3]. For example, TRF sunscreen in nanostructured lipid carrier has been proven for skin photoprotection to delay skin aging [4]. However, its practical use in dermatological products is limited due to its hydrophobic nature and high molecular weight which pose significant challenges for effective skin delivery [5]. Current research highlights the difficulty in achieving adequate skin penetration of TRF due to the barrier properties of the stratum corneum [6,7]. To address this limitation, there is a growing interest in developing innovative delivery systems that can enhance the topical delivery of TRF.

Proniosomal gel

Among the various strategies explored for enhancing topical delivery, the use of proniosomal gel (PNG) has shown considerable promise. PNGs are a derivative of niosomes,

*Corresponding Author
Chee Chin Chu, School of Pharmacy, Faculty of Health and Medical Sciences, Taylor's University, Subang Jaya, Malaysia.
E-mail: cheechin.chu @ taylors.edu.my

© 2025 Tanya Tong-en Fong *et al*. This is an open access article distributed under the terms of the Creative Commons Attribution 4.0 International License (https://creativecommons.org/licenses/by/4.0/).

composed in a gel form, that transform into niosomes upon hydration [8,9]. This transformation leverages the structural advantages of niosomes, such as the ability to encapsulate hydrophobic substances and facilitate their controlled release, while offering enhanced stability and ease of application characteristic of gel formulations [10]. Recent research has revealed the remarkable capabilities of PNG for delivering drugs through the skin. For instance, research on naproxen-loaded PNGs demonstrated a high entrapment efficiency (EE) of 92.33% with a formulation that includes Span® 60, lecithin, cholesterol, and ethanol developed through the coacervation-phase separation method [11]. Similarly, another study on PNG with active ingredient cilostazol showed controlled drug release profiles that significantly enhance drug flux in *ex vivo* studies [12]. Moreover, a study on tramadol-loaded PNGs formed stable, optimally-sized vesicles which facilitated prolonged drug release, enhancing the drug's therapeutic effects while reducing the need for frequent administration [13].

Terpenes

In addition to the structural benefits of PNGs, the integration of chemical penetration enhancers in vesicular delivery systems offers further enhancements in drug transport through the skin [6]. Natural terpenes like D-limonene and squalene are widely recognized as effective chemical penetration enhancers. By temporarily disrupting the skin barrier, they improve the permeability of active ingredients [14]. Moreover, their natural origin ensures minimal irritation or toxicity, aligning with the growing consumer demand for safe and natural cosmetic ingredients [15].

While the base composition of PNG formulations has been well established through previous research, the incorporation of terpenes into such systems remains largely unexplored. In contrast, terpenes have been extensively studied in invasomal systems, where they function as effective penetration enhancers by temporarily disrupting the stratum corneum to facilitate transdermal drug [16–18]. Addressing this research gap, the present study aims to incorporate selected terpenes such as D-limonene and squalene PNG formulations for the topical delivery of palm TRF. D-limonene and squalene were chosen due to their hydrophobic nature, which enhances compatibility with lipophilic compounds such as TRF [19]. Specifically, the study focuses on determining the optimal concentration of terpenes, followed by evaluating the physical characteristics, antioxidant activity, *in vitro* release, and release kinetics of the TRF-loaded PNG formulations.

MATERIALS AND METHODS

Materials

Span® 60, soy lecithin, cholesterol, absolute ethanol, methanol, squalene, limonene, Transcutol®, and 2,2-diphenyl-1-picrylhydrazyl (DPPH) were procured from Sigma-Aldrich (Munich, Germany). TRF (TRF 96% purity; d-α-Tocopherols, d-α-Tocotrienol, d-β-Tocotrienol, d-γ-Tocotrienol, d-***δ***-Tocotrienol, and d-***α***-Tocomonoenol) was obtained from KLK Oleo Sdn Bhd (Selangor, Malaysia). Sodium acetate buffer and phosphate buffer saline were purchased from Nacalai Tesque Inc. (Kyoto, Japan). The cellulose nitrate membrane having a size of 25 mm was procured from Whatman (0.45 nm pore size; Whatman, UK). The ultrapure water was produced by the Sartorius Stedim Biotech Arium 611DI system (Goettingen, Germany). Every chemical that was acquired was of analytical quality.

Methods

Preparation of PNG

TRF-loaded PNG was formulated utilizing the coacervation-phase separation method adapted from the previous study by Sakdiset *et al.* [20] with slight modifications. Table 1 shows the composition of formulations from Span® 60, soy lecithin, cholesterol, and phosphate buffer proposed by Tareen et al. [21]. The ratio of Span® 60 to soy lecithin was set at 1:1; the ratio of solvent to aqueous phase was 2:1; the ratio of Span® 60 to cholesterol was set at 9:1. On the other hand, the concentrations of D-limonene and squalene incorporated into the PNG formulations were selected based on established literature and the need to maintain a balance between efficacy and safety. Terpenes are commonly used as chemical penetration enhancers in topical formulations at concentrations ranging from 0.4% to 10%, with 0.5% to 5% being the most frequently used range to minimize the risk of skin irritation [22,23]. In this study, each terpene was incorporated individually at concentrations of 5% and 10%, while combinations of D-limonene and squalene were prepared

Table 1. Formulations of proniosomal gel.

Formulation code	Proniosomal gel composition (% w/w)				Solvent (% w/w)		Penetration enhancer (% w/w)		MCT oil (% w/w)
	Span® 60	Soy lecithin	Cholesterol	Phosphate buffer	Ethanol	TRF	d-limonene	Squalene	
Plain MCT 5%	22.7	22.7	2.5	20.2	31.5	0.4	-	-	5.0
Plain MCT 10%	22.7	22.7	2.5	20.2	31.5	0.4	-	-	10.0
D5	22.7	22.7	2.5	20.2	31.5	0.4	5.0	-	-
D10	22.7	22.7	2.5	20.2	31.5	0.4	10.0	-	-
S5	22.7	22.7	2.5	20.2	31.5	0.4	-	5.0	-
S10	22.7	22.7	2.5	20.2	31.5	0.4	-	10.0	-
M2.5	22.7	22.7	2.5	20.2	31.5	0.4	2.5	2.5	-
M5	22.7	22.7	2.5	20.2	31.5	0.4	5.0	5.0	-

using 2.5% and 5% of each terpene, respectively, to achieve total terpene concentrations of 5% and 10%. This selection falls within the recommended safe and effective range.

TRF was initially dissolved in ethanol using a vortex mixer to create a homogeneous solution and the vial was closed to prevent the solvent from evaporating. During the production of PNG, Span® 60, soy lecithin, and cholesterol were mixed in a glass vial with the TRF solution. The mixture was heated in a shaking water bath (Memmert WB 22/SV 1422, Memmert GmbH & Co. KG, Germany) at 65°C ± 1°C until complete solubility was attained. Subsequently, the terpenes and phosphate buffer were introduced into the molten mixture. The mixture was then placed in the shaking water bath again until complete solubility was acquired. The final proniosomal dispersion was allowed to cool until it solidified into gels. The prepared PNG was stored in the same vial at 4°C for further characterization. Similarly, control formulations consisted of negative controls [TRF-loaded PNG without terpene but replaced with medium chain triglyceride (MCT) (Plain MCT 5% and Plain MCT 10%)], positive control (Transcutol® 10%), and sample control (PNG with terpene but without TRF (Plain w/o TRF)) were prepared for comparison purposes.

Reconstitution of PNG into niosomal dispersion

To reconstitute the PNG into niosome for further characterization, every 0.1 g sample was reconstituted with 9.9 ml of ultrapure water in a centrifuge tube [11].

Particle size and polydispersity index

The Zetasizer Nano ZS (Malvern Panalytical, Malvern, UK) was used to measure the mean particle size and polydispersity index (PDI) using dynamic light scattering at 25°C. Before the measurements, the PNG was reconstituted into niosome with ultrapure water in a 100-fold dilution factor. It was subjected to bath sonication for 30 minutes (Elmasonic S 180 H, Elma Schmidbauer GmbH, Germany) to obtain the homogenous TRF-loaded niosomal solutions. A disposable capillary cuvette DTS1060 with electrodes (Malvern Panalytical, Malvern, UK) was then used to measure the niosome in triplicate [20,24].

Entrapment efficiency

The EE was determined by the centrifugation method adapted from El-Enin *et al.* [25] and Gentili *et al.* [26] with slight modifications. About 0.1 g of PNG was dissolved in 9.9 ml of ethanol and was then centrifuged using a centrifuge (UNIVERSAL 320 centrifuge, Hettich Andreas Hettich GmbH & Co. KG, Germany) with a rotor radius of 8.5 cm, generating a relative centrifugal force of approximately 7692 × g at 9,000 rpm for 30 minutes at 25°C. The supernatant was collected and assayed by using a UV-Vis spectrometer (Secomam Uviline 9600 UV/Visible spectrophotometer, Secomam Aqualabo Group, UK) to measure the absorbance at 295 nm. The concentration of the TRF in the samples was calculated over a standard curve of TRF in ethanol from the concentration range of 0.03–300 ppm with calibration equation of $y = 7.1829x + 0.0237$ with $R^2 = 0.9999$. The samples' EE was determined using the following formula:

$$EE\% = \frac{T_t - T_f}{T_t} \times 100 \quad (1)$$

where T_t represents the total amount of TRF included in the PNG, and T_f denotes the unentrapped TRF amount present in the supernatant.

Antioxidant activities

Free radical DPPH was used for assessing the antioxidant activity of PNG with protocols according to the previously described method [27]. An amount of 0.1 ml of diluted sample in denatured ethanol was added into a test tube followed by 3.9 ml ethanolic DPPH solution with every sample was done in triplicate. Following the addition of DPPH, the samples were incubated for 30 minutes. The UV-Vis spectrophotometer was used to measure the optical density at 517 nm against an ethanol blank (Secomam Uviline 9600 UV/Visible spectrophotometer, Secomam Aqualabo Group, UK). The antioxidant activity of the PNG was reported as mg Trolox equivalents per gram of sample (mg TE/g sample) over a standard curve of Trolox prepared from the concentration range of 0.02–0.10 mg/ml with a calibration equation of $y = -7.105x + 1.4027$ with $R^2 = 0.9664$.

Optimization of the formulation

The formulation that indicated the highest EE for TRF and antioxidant activity (M5) was selected to proceed for further analyses and compared with the control formulations to evaluate the specific contributions of various components. Negative control included TRF-loaded PNG without terpenes but replaced with MCT (Plain MCT 5% and Plain MCT 10%) to assess the effect of terpenes on the encapsulation and activity of TRF-loaded PNG. The positive control (Transcutol® 10%) was included to compare the effects of a known penetration enhancer with the optimized M5 formulation containing 10% terpenes. A sample control, PNG with terpenes but without TRF (Plain w/o TRF), was also prepared to evaluate the impact of terpenes on the formulation independent of TRF.

Fourier-transform infrared spectroscopic analysis

The Fourier-transform infrared (FTIR) analysis was performed using Fourier transform infrared spectroscopy (Thermo Fisher Scientific, USA) to assess the compatibility of PNG's ingredients and formulations. Thirty-two scans were conducted at room temperature with a spectral resolution of 4 cm^{-1} in the range of 600–4,000 cm^{-1} [24].

Rheological behavior

The rheological behavior of the optimized sample (M5) and control samples was studied with slightly modified protocols following the previously reported method [28]. A rheometer (MCR 102e, Anton Paar, Graz, Austria) with measuring plate (PP25/SP; D: 25 mm) was used to measure the samples' rheological behavior. The compartment was filled with a suitable quantity of sample at the rheometer plate's center with the gap set at 0.5 mm. The rotational test of the samples was conducted while scanning the PNG at a shear rate

of 0.01–100 s^{-1}. Further, oscillatory tests were conducted over a strain sweep of 0.001%–50% strain, at an angular velocity of 10 rad/s and 37°C to identify the linear viscoelastic area. The elastic modulus (G′) and viscoelastic modulus (G″) of the PNG were then measured by performing a frequency sweep of 0.1–100 rad/s in the linear viscoelastic region with 0.1% strain selected. The data were collected and analyzed by RheoCompass (Anton Paar, Germany) to determine the non-linear parameters to determine the flow and rheological properties, predicting the stability of the samples.

Thermal stability and crystallinity

The thermal properties of the ingredients and samples were examined using differential scanning calorimetry (DSC) (DSC1 STARe System, Mettler Toledo, USA) to detect the melting point differences between the pure ingredients and the formulation created. The test was conducted according to the slightly modified method of Lasó *et al.* [20]. The precisely weighed samples at 10 mg were added to an aluminum pan and crimped. The analysis was conducted at temperatures between −4°C and 170°C using a uniform heating increment rate of 10°C/min under a nitrogen atmosphere with a 20 ml/min nitrogen flowing rate [29].

In vitro release profile of palm TRF

The *in vitro* release profile of TRF was studied using the Franz diffusion cell (Diffusion Cell Apparatus Model EDC-07, Electrolab, India) following a previously reported method [30] with slight modifications. The receptor medium was prepared using phosphate-buffered saline (PBS), pH 5.5, and ethanol at 70:30, v/v. The donor chamber and the receptor chamber were separated by a 25 mm cellulose nitrate membrane (0.45 nm pore size; Whatman, UK). About 600 mg of the sample was then placed on the hydrated cellulose membrane. To prevent medium evaporation, parafilm was used to cover the donor and recipient compartment openings. After that, about 600 mg of the sample was placed on the moistened cellulose membrane. To stop medium evaporation, parafilm was placed over the donor and recipient compartment openings. Water was circulated through an external water jacket to keep the assembly at 37°C ± 0.5°C, and the receptor medium was continuously stirred at 400 rpm. At 0.5, 1, 2, 3, 4, and 6 hours, 1 ml of the samples was withdrawn from the receptor chamber and replenished with 1 ml buffer solution. The collected samples were examined in triplicates using the microplate reader (SPECTROstar Nano Microplate Reader, BMG Labtech, Germany) at 295 nm and the amount of drug released was calculated by utilizing the standard curve of TRF in the ethanol buffer solution prepared from the concentration range of 20–313 ppm with calibration curve y = 0.0006x + 0.0189 with R^2 = 0.994. The mean cumulative amount of drug release was graphed over time and the release kinetics of TRF from PNG was further studied by fitting the data of drug release to different kinetic models such as zero-order, first-order, Higuchi, Korsmeyer–Peppas, and Hixson–Crowell diffusion models using formulas as follows [31]:

$$\text{Zero-order model: } Q = Q_0 + kt \quad (2)$$

$$\text{First-order model: } Q = Q_0 \times e^{kt} \quad (3)$$

$$\text{Higuchi model: } Q = k \times t^{0.5} \quad (4)$$

$$\text{Hixson–Crowell model: } Q^{1/3} = kt + Q_0^{1/3} \quad (5)$$

$$\text{Korsmeyer–Peppas model: } Q = k \times t^n \quad (6)$$

where Q denotes the quantity of TRF released in time t, Q_0 represents the value of Q at zero time, k represents the rate constant, n represents the diffusional exponent, a represents the time constant, and b represents the shape parameter. The coefficient of determination (R^2) was used to choose the model that best fits the experimental result. The Korsmeyer–Peppas kinetic model was used to determine the release mechanism of TRF from the PNG based on the value of release coefficient (n) calculated by linear regression ($n \leq 0.5$ = Fickian diffusion, $0.5 < n \leq 0.9$ = non-Fickian transport, and $n \leq 0.9$ = case-II transport) [32].

Statistical analysis

All the measurements were performed in triplicate (n = 3) with the results reported as mean ± SD. The results were analyzed using a one-way analysis of variance with Tukey's *post hoc* test to identify any significant differences at a 95% confidence interval (CI) ($p < 0.05$). MINITAB 17 (Minitab, Inc., State College, PA) statistical software was used to analyze all the results.

RESULTS AND DISCUSSION

Particle size and PDI

The particle size of the proniosomal formulations ranged from 271.60 ± 30.10 nm to 416.40 ± 7.62 nm (Table 2). Maintaining nanoscale particle sizes is beneficial for topical delivery as it promotes closer interaction with the stratum corneum and enhances skin permeation [33]. The particle sizes were consistent with a previous study from Shah *et al.* [11] using a similar base composition comprising Span 60 (1,800 mg), lecithin (1,800 mg), and cholesterol (20 mg). This similarity in formulation base suggests that the addition of terpenes in the present study did not markedly influence the particle size of the proniosomal formulations. The homogeneity of the particle size distribution was ascertained by calculating the PDI. The value of the PDI typically falls between 0 and 1, with values less than 0.1 denoting monodispersity and values more than 0.3 denoting substantial heterogeneity or polydispersity [11]. Table 2 indicates that most formulations exhibited intermediate PDI values (0.1–0.3) with relatively narrow particle size distribution. A few formulations such as M2.5, M5, and plain w/o TRF had PDI values slightly exceeding 0.3, indicating a slightly more diverse size range. However, there was no significant difference in the PDI among the studied formulations with different types of terpenes and concentrations used.

The influence of the addition of terpenes on the particle size of formulations was significant ($p < 0.05$). Terpenes at 5% concentration (i.e., D5 and S5) resulted in significantly smaller particle sizes compared to Plain MCT 5%. This phenomenon

Table 2. Particle size, PDI, EE and antioxidant activities of the proniosomal gels.

Formulation	Particle size (nm)	PDI	EE (%)	Antioxidant activities (mg TE/g sample)
Plain MCT 5%	354.30 ± 31.20^{bc}	0.198 ± 0.092^{a}	98.328 ± 0.024^{b}	0.193 ± 0.014^{e}
Plain MCT 10%	272.57 ± 12.29^{d}	0.203 ± 0.023^{a}	98.081 ± 0.013^{cd}	0.215 ± 0.002^{e}
D5	271.60 ± 30.10^{d}	0.142 ± 0.152^{a}	98.530 ± 0.048^{a}	2.112 ± 0.035^{c}
D10	318.90 ± 24.60^{cd}	0.269 ± 0.214^{a}	98.442 ± 0.002^{ab}	2.059 ± 0.035^{c}
S5	314.83 ± 16.03^{cd}	0.180 ± 0.050^{a}	98.161 ± 0.038^{c}	2.262 ± 0.042^{c}
S10	282.23 ± 0.90^{d}	0.190 ± 0.022^{a}	98.006 ± 0.030^{e}	2.122 ± 0.049^{c}
M2.5	416.40 ± 7.62^{a}	0.311 ± 0.069^{a}	98.443 ± 0.031^{ab}	2.647 ± 0.035^{b}
M5	364.53 ± 2.32^{bc}	0.382 ± 0.016^{a}	98.471 ± 0.116^{a}	2.951 ± 0.028^{a}
Plain w/o TRF	398.07 ± 1.85^{ab}	0.354 ± 0.022^{a}	-	-
Transcutol® 10%	380.80 ± 3.15^{ab}	0.284 ± 0.030^{a}	97.925 ± 0.00^{9}e	0.648 ± 0.283^{d}

Data were presented as means ± SD (n = 3). Different superscript letters (^{a,b,c,d,e,f,g}) indicate significant differences (Tukey, $p < 0.05$; CI: 95%) within each column.

may be attributed to the impacts of D-limonene and squalene which can enhance the membrane fluidity and reduce interfacial tension. This ultimately prevented droplet agglomeration and formed smaller vesicles [34]. Similar observations were reported using nanoemulsions with the different concentrations of D-limonene [35]. However, this effect was not observed at higher concentrations (10%) as both D10 and S10 had no significant difference from plain MCT 10%. This may be due to competing mechanisms at elevated terpene levels. While low terpene concentrations (5%) effectively reduce interfacial tension and inhibit droplet coalescence, higher concentrations (10%) may increase the solubility of the oil phase, accelerating molecular diffusion (Ostwald ripening) and counteracting initial particle size reduction. Thus, the lack of further size reduction at 10% suggests a threshold beyond which terpenes no longer suppress droplet coalescence and may instead promote instability mechanisms such as Ostwald ripening [36].

The formulations containing both D-limonene and squalene (i.e., M2.5 and M5) had significantly larger particle sizes than all other formulations. It is apparent that the particle size increased with the increasing EE. Data from Table 2 were in good correlation with this observation, as M2.5 and M5 achieved EE of 98.443% ± 0.031% and 98.471% ± 0.116% corresponded to their larger particle size of 416.40 ± 7.62 and 364.53 ± 2.32 nm, respectively. The larger-sized particles could be formed when there was a higher loading of TRF within the hydrophobic area of the vesicle which likely caused an expansion and subsequent separation of the bilayer molecules. This is supported by studies suggesting a direct correlation between particle size and EE [11,13].

Entrapment efficiency

Table 2 shows that the overall EE for all formulations was within a narrow range of 97.925% ± 0.009%–98.530% ± 0.048%. This showed the constant high capacity of PNGs to capture the TRF. In addition to the effectiveness of the formulation, EE reflects the ability of a formulation to retain the active compound which can significantly influence the drug's release behavior in which a higher EE contributes to a delayed release rate [37]. The *in vitro* release profile of M5 as shown in Figure 4 was in good correlation with this observation. The initial release from M5 was low and slow due to the encapsulation of TRF within the niosomal bilayers which acted as a strong barrier to drug release. This suggests that the formulation allowed for a more controlled and steady release over time. The high EE values also suggest potential benefits for long-term stability. As most of the TRF was retained within the bilayers of the vesicles, it was likely protected from environmental factors such as oxidation and hydrolysis which in turn can prolong shelf life [38,39].

The influence of the type and concentration of terpenes used on the EE of the formulations was significant ($p < 0.05$). Formulations comprising only D-limonene (i.e., D5 and D10) consistently showed better EE than those containing only squalene or MCT oil. This phenomenon could be due to the presence of D-limonene ($C_{10}H_{16}$) is a monoterpene that has a small cyclic molecule. It can easily integrate into the lipid bilayer, thus increasing the membrane fluidity and reducing the surface tension in the vesicle. This resulted in better retention of TRF within the vesicles leading to the high EE in D5 and D10 samples (Table 2) [35,40].

On the other hand, squalene being a triterpene ($C_{30}H_{50}$) that has a larger and more complex linear structure showed reduced EE compared to both D-limonene formulations and plain MCT, particularly at higher concentrations. Unlike D-limonene, squalene's bulky structure may not integrate as effectively into the bilayer. Instead, its presence could create molecular packing disruptions in the vesicle structure, potentially leading to increased void spaces and reduced TRF retention capacity [41]. Formulations with higher concentrations of both D-limonene and squalene at higher concentrations (i.e., M5) exhibited higher EE than the Plain MCT 10% sample, while this effect was not evident at lower concentrations (i.e., M2.5). This suggests that while squalene can cancel the positive impact of D-limonene at lower concentrations, higher levels of D-limonene are capable of overcoming these destabilizing effects. The positive control Transcutol® 10% sample was found to have the lowest EE, suggesting that D-limonene and squalene were superior penetration enhancers for enhancing EE in comparison to the positive control.

Antioxidant activities

The high EE of all formulations indicates that the majority of the TRF was successfully encapsulated within the PNG matrices. Despite the high and similar EE values across all formulations, there was a notable difference in antioxidant activity. This suggests that factors beyond EE have a greater impact on the antioxidant properties of the formulations. For instance, D5 (98.53% EE) and M5 (98.47% EE) showed comparable encapsulation but differed markedly in antioxidant activity (2.112 and 2.951 mg TE/g; $p < 0.05$). Table 2 demonstrates that all formulations with terpenes exhibited 1.4- to 2.2-fold higher antioxidant activity than plain PNG controls with statistically significant differences ($p < 0.05$ for all comparisons against control). The plain PNGs, which were formulated with TRF but without terpenes, served as the control to evaluate the baseline antioxidant activity of TRF. The observed enhancement in antioxidant activity in the terpene-containing formulations may be attributed to the intrinsic antioxidant chemical properties of the terpenes which likely act synergistically with TRF to improve the overall antioxidant capacity of the formulation. For instance, D-limonene acts as a good antioxidant agent by donating hydrogen atoms or electrons to neutralize free radicals [42], while squalene also acts a potent antioxidant by quenching singlet oxygen and preventing lipid peroxidation [43]. The formulations comprising a mix of D-limonene and squalene (i.e., M2.5 and M5) exhibited the best antioxidant activity of all formulations likely due to their synergistic effects. These terpenes have different mechanisms of antioxidant action and can result in a cumulative antioxidant effect. Similar findings were reported by Ortiz *et al.* [44] that proved the combinations of essential oil terpenes can exhibit enhanced antioxidant activity compared to individual terpenes.

On the other hand, there were no significant differences observed in antioxidant activity between different types of terpenes and concentrations when they were used alone. The lack of significant differences in antioxidant activity with individual use of terpenes at higher concentrations suggested that each terpene might have reached a saturation point, beyond which increasing its concentration further did not significantly increase the antioxidant capacity The saturation effect can be explained by several mechanisms: (1) limited solubility or incorporation capacity of the vesicle system, (2) potential self-aggregation of terpene molecules at high concentration that reduces their effective surface area for antioxidant activity, and (3) limited availability of reactive oxygen species to interact with the antioxidants at higher terpene concentrations [45–47]. Thus, the results suggested that the increased antioxidant activity in the terpenes-added formulations could be due to the intrinsic and synergistic properties of D-limonene and squalene, with higher concentrations enhancing effects until a saturation point is reached. The positive control with 10% Transcutol® had lower antioxidant activity than the terpene-added formulations, implying that both terpenes had greater antioxidant capabilities than the positive control.

FTIR spectroscopic analysis

The spectra of all formulations using various raw materials are shown in Figure 1a–d. The FTIR analysis of Span® 60 showed characteristic peaks at 3,395 cm^{-1} of –OH stretching of carboxyl group, at 2,915 and 2,848 cm^{-1} of –CH stretching of alkane, and in 1,730 and 1,467 cm^{-1} of –C=O bond of ester as functional groups. The cholesterol showed peaks at 3,423 cm^{-1} of carboxyl group, at 2,930 and 2,865 cm^{-1} of –CH stretching of alkane, and at 1,647 cm^{-1} of variable alkene –C=C stretching. TRF showed plenty of prominent FTIR peaks, including 3,410 cm^{-1} of–OH stretching of carboxyl group, 2,923 and 2,853 cm^{-1} of –CH stretching of alkane, 1,618 and 1,716 cm^{-1} of –C=C stretching, 1,448 cm^{-1} of –CH bend, and 1,376 cm^{-1} of –C–C stretch.

As shown in Figure 1c and d, all the formulated samples also had similar characteristic bands in the spectra region, indicating that the base components of the PNG and TRF were successfully incorporated in all samples. For instance, peaks associated with –OH stretching (~3,423, ~3,410, ~3,300 cm^{-1}) in the ethanol, TRF, and cholesterol were consistently detected in all samples. Similarly, characteristic peaks corresponding to –C=O bonds (~1,730, ~1,647 cm^{-1}) in Span® 60 were present in all formulations except D10 and S5. Setiadi and Hidayah [48] reported the FTIR equipment is capable of demonstrating the removal of a single fatty acid chain from the structure. They identified the fatty acids from the lecithin structure at wave numbers of 3,605 cm^{-1} of –OH stretching of carboxyl group, 1,619 cm^{-1} of alkene –C=C stretching, 1,088 cm^{-1} of –C–C stretching and 657 cm^{-1} of –CH bending. All formulated samples showed similar characteristic peaks of soy lecithin –C–C stretching and –CH bend indicating no breaking of a single fatty acid chain.

The FTIR spectra analysis of the proniosomal formulations showed significant shifts in the −OH stretching bands, particularly in formulations with squalene (i.e., S5, S10, M2.5, and M5). Notably, the –OH peak of TRF (3,410 cm^{-1}) showed a 12 cm^{-1} redshift in D-limonene containing formulations (D5/D10) versus only 5 cm^{-1} in squalene containing samples (S5/S10), suggesting preferential H-bonding between D-limonene and TRF's phenolic groups that may enhance the oxidative stability of TRF. This effect can be attributed to squalene's integration into the midplane of the lipid bilayer, where it disrupts intermolecular hydrogen bonding networks [41]. D-limonene in D5 and D10 primarily formed hydrogen bonding interactions with other components in the formulations. When hydrogen bonding occurred, the −OH group was no longer free and led to a lengthening of the −OH bond and a corresponding decrease in the stretching frequency [49]. On the other hand, the high concentration of D-limonene in D10 could lead to a very fluid and disordered membrane structure, which would cause the −C=O bonds to vanish from the spectra and produce the greatest shifts of −OH peaks. The absence of the −CH bending peak in D10 implied that the large D-limonene concentration exceeded the lipid bilayer's saturation capacity which can induce complete fluidization of lipid membrane causing alterations in the acyl chain packing which eliminate symmetric −CH bending vibrations [50]. Furthermore, the FTIR study showed no major new peaks or bond formations after encapsulation, suggesting that the encapsulated TRF maintained its molecular structure without any major chemical changes [51].

Rheological behavior

As shown in Figure 2a, the rheological analysis of all the PNG formulations revealed a non-Newtonian, shear-

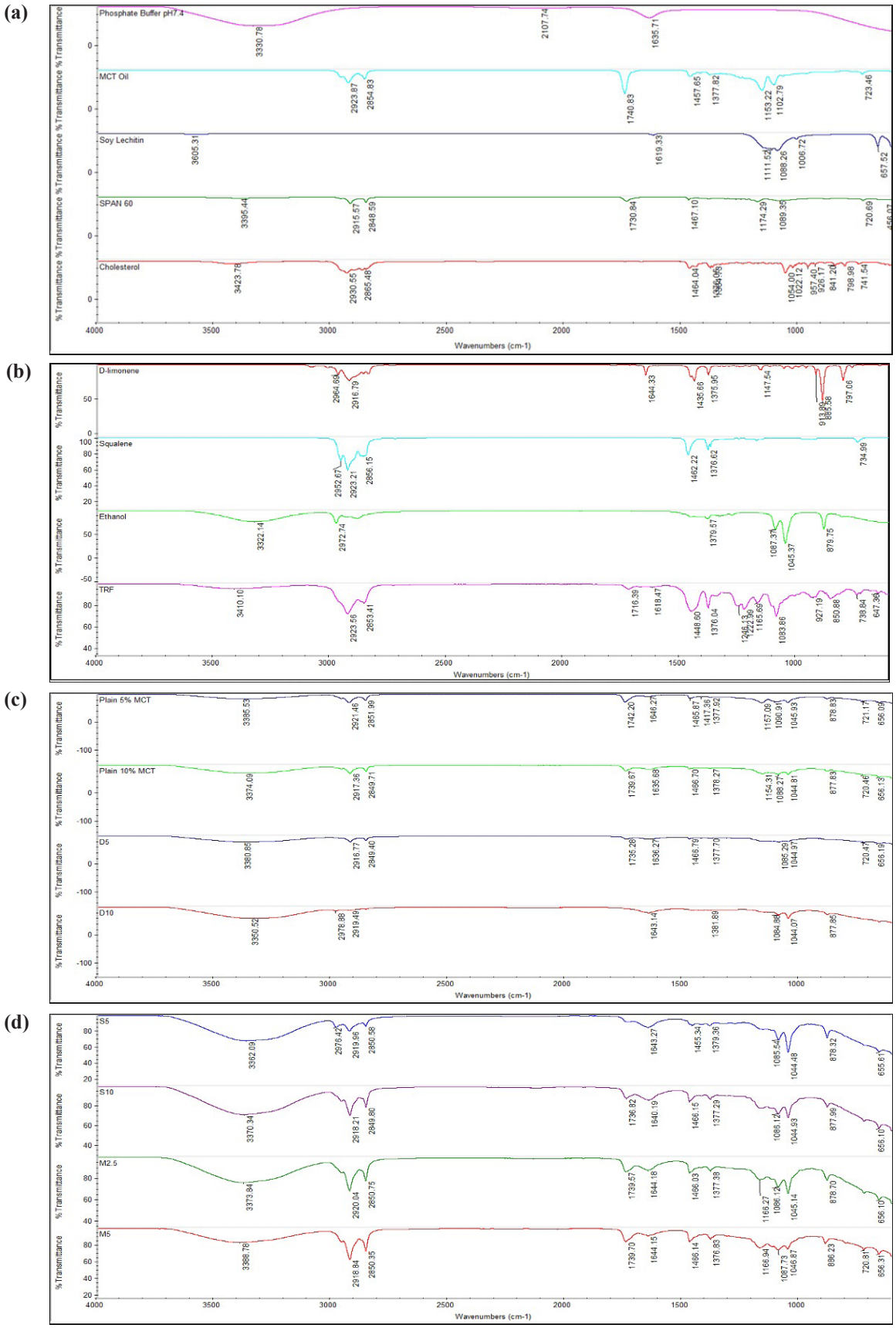

Figure 1. FTIR spectra for (a, b) raw materials and (c, d) samples. D5 = PNG produced from 5% D-limonene; D10 = PNG produced from 5% D-limonene; M2.5 = PNG produced from a mixture of 2.5% D-limonene and 2.5% squalene; M5 = PNG produced from a mixture of 5% D-limonene and 5% squalene; MCT = medium chain triglyceride; S5 = PNG produced from 5% squalene; S10 = PNG produced from 10% squalene; TRF = tocotrienol-rich fraction.

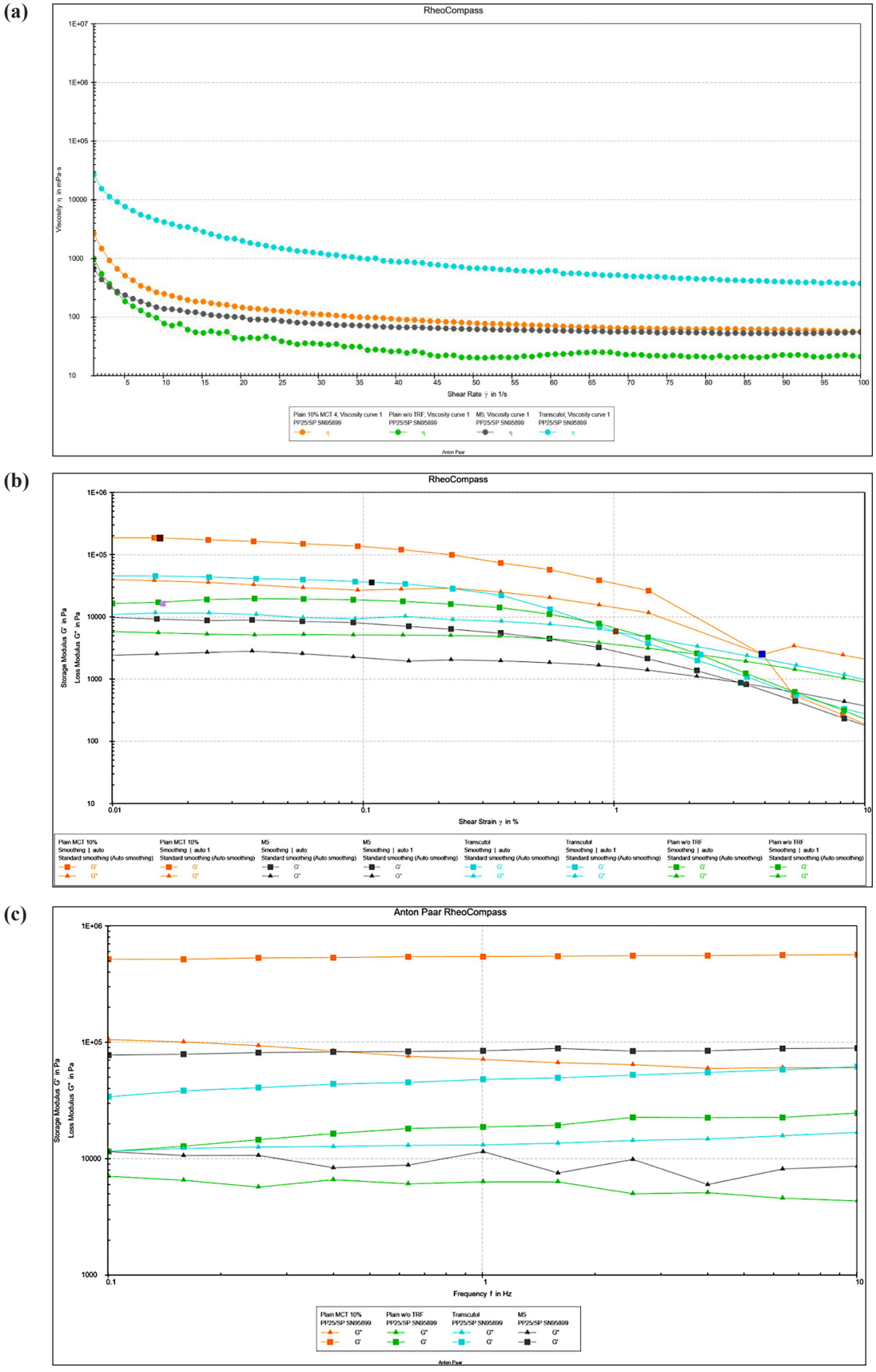

Figure 2. (a) Effect of different proportions of PNGs on samples' viscosity; (b) elastic modulus (G′) and viscous modulus (G″) of samples under 0.01%–100% strain conditions; (c) elastic modulus (G′) and viscous modulus (G″) of samples at 0.1–10 Hz. M5 = PNG produced from a mixture of 5% D-limonene and 5% squalene; MCT = medium chain triglyceride; TRF = tocotrienol-rich fraction.

thinning behavior which is characterized by a decreasing viscosity with the increasing shear rate. This flow behavior of PNG is favorable as it facilitates easy application including smooth spreading on the skin surface and squeezing the product out of the packaging [52]. Similar shear-thinning flow behavior was also observed in other studies on PNGs [22,53]. According to the result from regression analysis focused on fitting the data to various rheological models, the data fitted best into the Herschel–Bulkley equation with the highest R^2 value of 0.9999. The data retrieved from the model were consistent with the shear-thinning flow that is observed when a stress exceeded the yield stress, and the results were consistent with a previous study [12]. The addition of D-limonene and squalene in M5 sample contributed to the lowest initial viscosity compared to all other control formulations. This could be attributed to the presence of D-limonene and squalene in M5 which can fluidize the lamellar structure of PNG and reduce the rigidity of the lipid bilayer resulting in lower viscosity [54]. Lasó et al. [20] reported similar findings, where lower viscosity was observed for PNGs containing D-limonene compared to plain PNG formulations.

Figure 2b shows the changes in the elastic modulus (G′) and viscous modulus (G″) of the samples which determined the conditions for frequency scanning. In the linear viscoelastic range, all PNG samples behaved predominantly like solids with the elastic modulus (G′) being greater than the viscous modulus (G″), which further indicated the samples exhibited the characteristics of a viscoelastic solid and possessed a certain level of physical stability when at rest. As the strain increased, G′ and G″ decreased and eventually intersected at a crossover strain beyond which the point, strain G″ exceeded G′, indicating a dominant viscous response. Two more parameters were acquired from amplitude sweep in Figure 2b: (1) yield stress, as the last shear stress value of at the limit of non-destructive linear viscoelastic (LVE) range that is the range beyond which the system begins to flow and (2) flow point, as the shear stress value where G′ = G″, indicating the transition from solid-like to liquid-like behavior. These measurements control product performance, in which an optimal yield stress allowing product stays stable in storage yet dispenses easily with gentle pressure, and an ideal flow point ensures smooth spreadability upon application [55]. M5 sample (0.005%) exhibited the lowest yield point value than those of Plain MCT 10% (0.016%) and Plain w/o TRF (0.016%) and Transcutol® 10% (0.106%). This may be attributed to the molecular changes resulting from the addition of terpenes in the M5 sample which can affect the intermolecular networks in the gel structure [35]. Despite its low yield point, the M5 sample had a relatively high flow point at 3.204%, which was higher than those of Transcutol® 10% (1.017%) and the Plain w/o TRF sample (2.215%) but was lower than Plain MCT 10% with flow point observed at 3.894%. This means that even though M5 began to deform at a low strain, it did not switch to fluid-like behavior until a greater strain was attained. The mechanism of the structural deformation was not examined in this study. However, the observation suggested that the network structure formed with terpenes (M5) could be more resilient, allowing the gel to withstand greater deformation before significant flow occurs. This combination implies that M5 is easy to spread under user pressure yet stable enough to maintain its structure during storage. This resilience might come

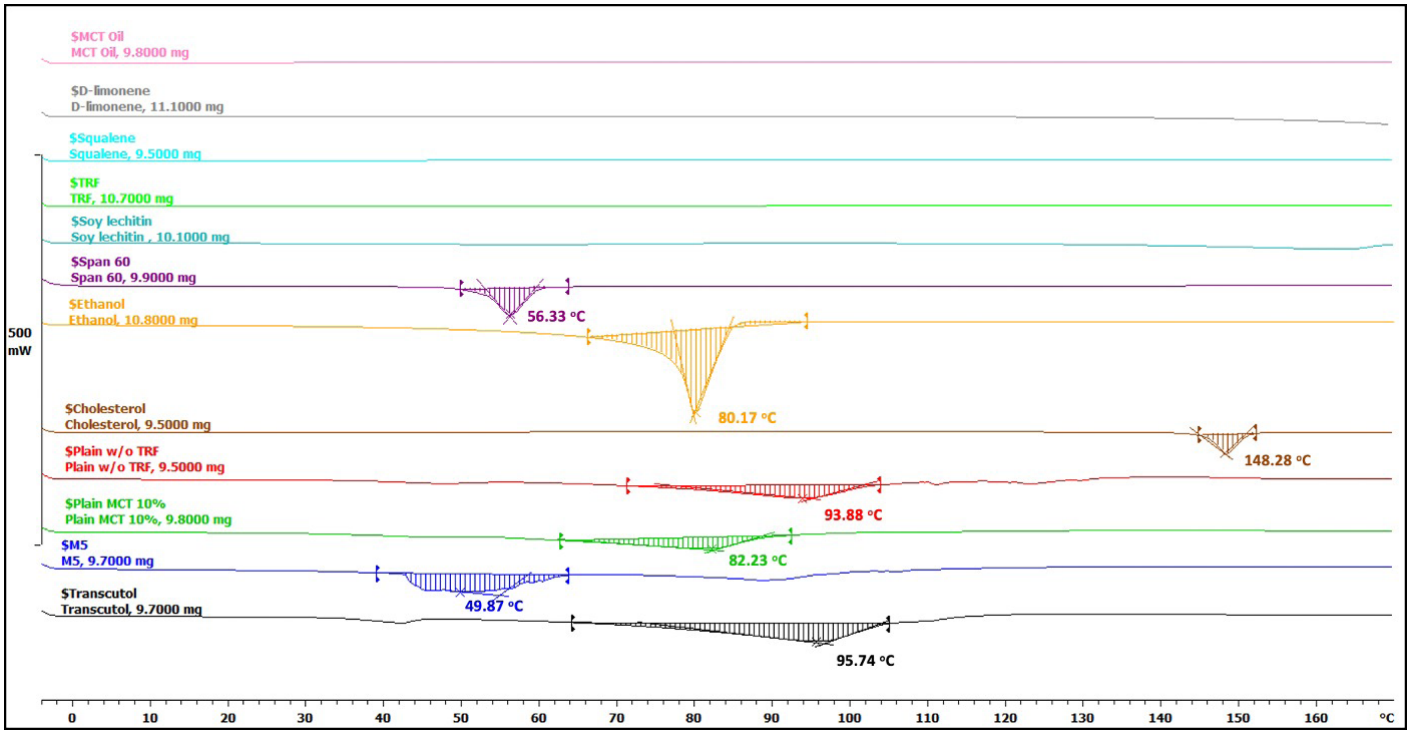

Figure 3. DSC patterns of the raw materials and samples. M5 = PNG produced from a mixture of 5% D-limonene and 5% squalene; MCT = medium chain triglyceride; TRF = tocotrienol-rich fraction.

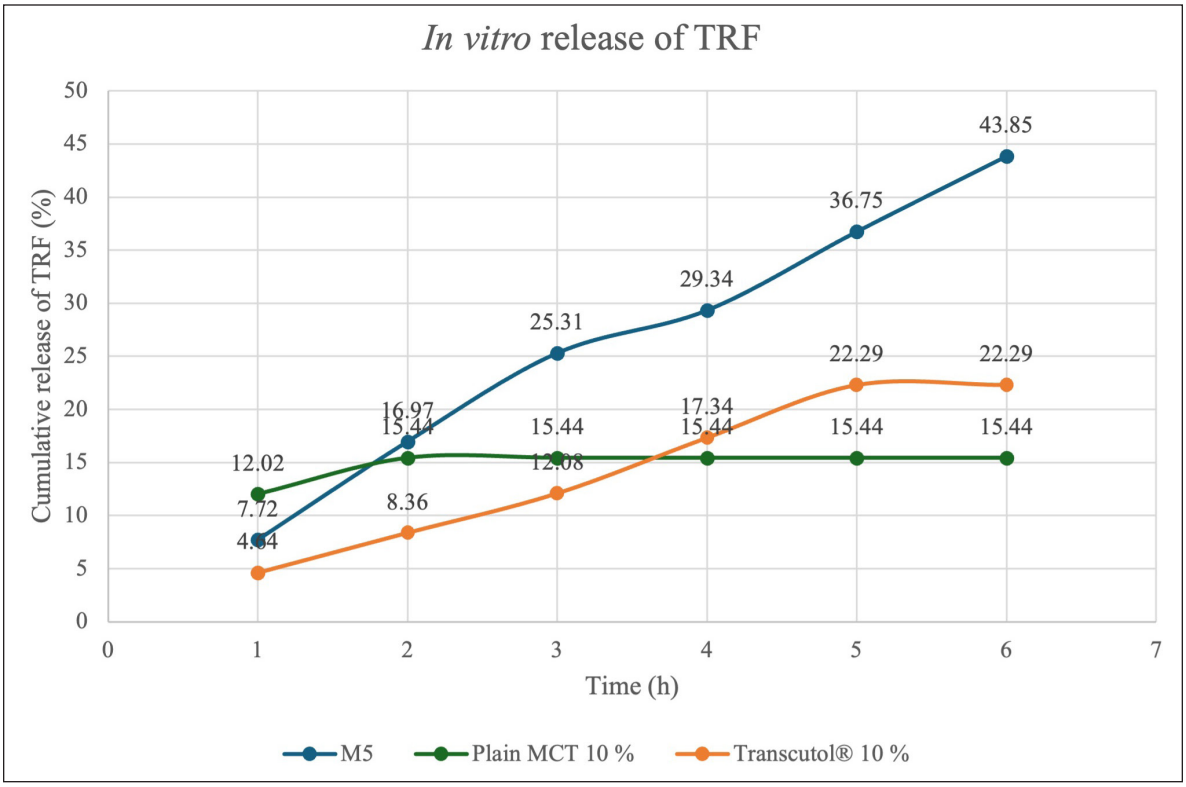

Figure 4. Comparison of percentage of TRF release from optimized sample and control samples. M5 = PNG produced from a mixture of 5% D-limonene and 5% squalene; MCT = medium chain triglyceride; TRF = tocotrienol-rich fraction

Table 3. Summarized drug-release kinetics modelling data for M5, Transcutol® 10%, and Plain MCT.

Sample	Zero order	First order	Higuchi	Hixson–Crowell	Korsmeyer–Peppas	
	R^2	R^2	R^2	R^2	R^2	n
M5	0.9387	0.7720	**0.9877**	0.8383	0.9645	-
Transcutol® 10%	0.8814	0.7945	0.9468	0.8326	**0.9742**	0.6632
Plain MCT 10%	0.2910	0.2910	0.4111	0.2910	**0.5579**	0.0826

Bold values denote the highest R^2 values across all models.

from the ability of terpenes to stabilize the gel system through hydrophobic interactions or other molecular mechanisms.

The frequency sweeps, which describe the time-dependent behavior in the LVE range, were employed in addition to characterize the internal structure at rest and both the short- and long-term storage stability of the developed PNGs [52,55]. Given that frequency is the reciprocal of time, greater frequencies reveal the short-term dispersion characteristics, such as rapid motion during transportation. On the other hand, lower frequencies provide information about the long-term behavior, such as stability against sedimentation, flotation, syneresis, and phase separation during storage [56]. Figure 2c illustrates the changes in the storage modulus (G′) and loss modulus (G″) across a range of frequencies. G′ consistently exceeds G″ in all samples suggesting the existence of three-dimensional network forces and indicates the building of the physical network structure [55]. All tested samples could be characterized by a relatively constant structural change with no crossover observed at both the lowest and highest frequency. These observations further presumed good structural rigidity at rest and both the short- and long-term storage stability. Specifically, the G′ value of M5 sample and Plain MCT 10% sample remained relatively constant with decreasing frequency suggesting their greater stability at rest or long-term storage stability than the plain PNGs formulations that contained without TRF (i.e., Plain w/o TRF) and the positive control sample that included 10% Transcutol® (i.e., Transcutol). This comparable observation between M5 and Plain MCT 10% formulation also showed that the addition of D-limonene and squalene did not affect the long-term stability of the PNGs.

DSC analysis

The DSC thermograms of the raw materials, M5 sample, as well as control samples including Transcutol® 10%, Plain MCT 10%, and Plain w/o TRF samples are presented in Figure 3. The melting points of Span® 60, ethanol, and cholesterol were

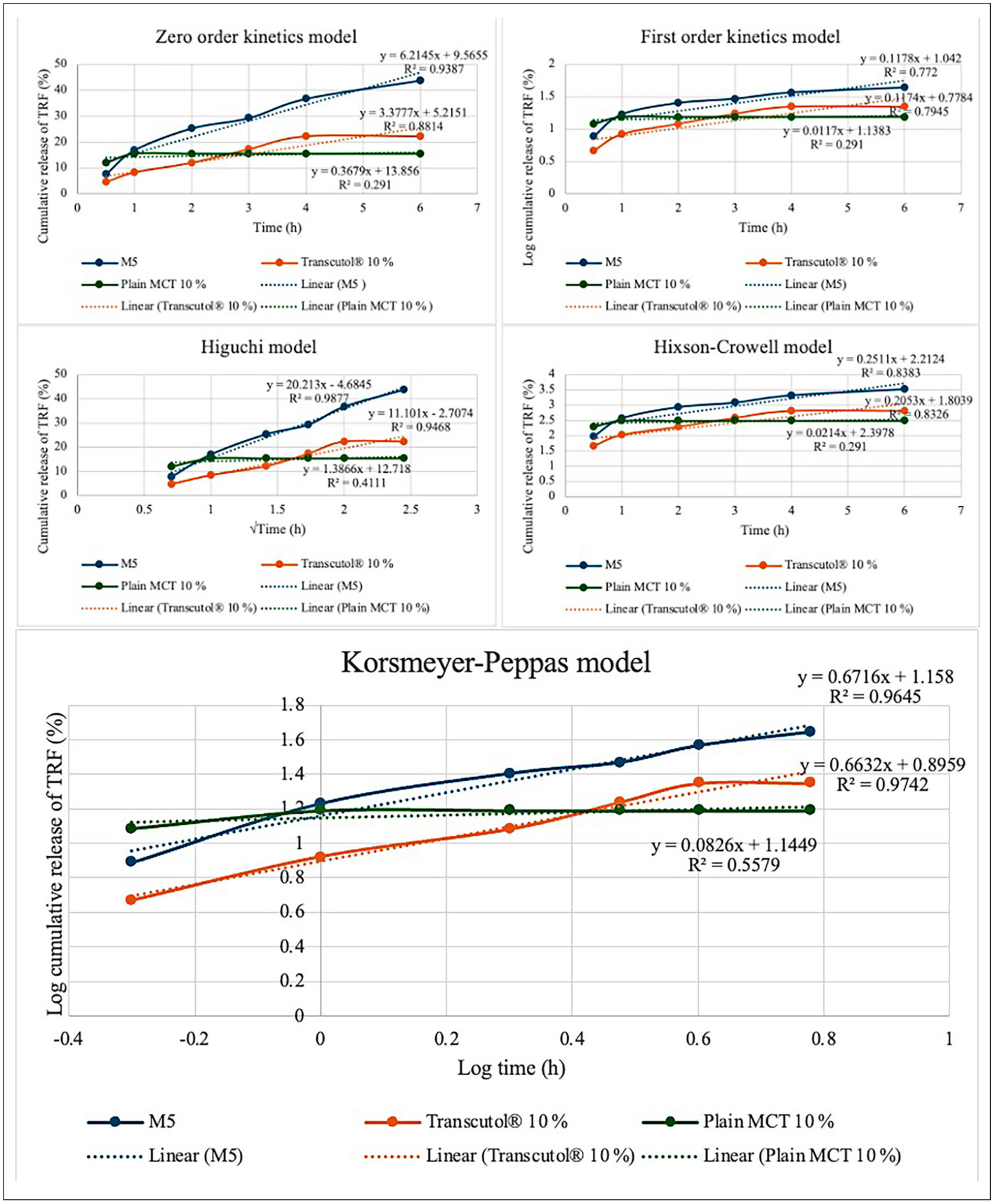

Figure 5. TRF release kinetics and mechanism from optimized sample and control samples. M5 = PNG produced from a mixture of 5% D-limonene and 5% squalene; MCT = medium chain triglyceride; TRF = tocotrienol-rich fraction.

at 56.33°C, 80.17°C, and 148.28°C, respectively. No distinct endothermic peaks were observed for MCT oil, D-limonene, squalene, TRF, and soy lecithin. This could be attributed to their liquid nature at room temperature, and thus they did not exhibit significant thermal transitions under the tested conditions. The thermograms of all the formulated samples showed significant broadening and shifting of endothermic peaks in comparison to the raw materials. The shifted melting endotherm of cholesterol in all tested samples signified that all the lipid components interact with each other to a great extent while forming the lipid bilayer. These results confirmed the formation of the double-layer structure of the vesicle [22]. The broadening typically resulted from the formation of a molecular dispersion. The results confirmed that the components are integrated at the molecular level within the bilayer, leading to a range of melting points rather than a single sharp peak [57]. Both D-limonene and squalene are terpenes known for their ability to disrupt lipid bilayers and enhance permeability. Their presence in the M5 sample likely led to significant disruption of the crystalline structure of the lipid components, resulting in a lower melting point at 49.87°C due to decreased intermolecular forces. This aligns with the findings of Schreier and Bouwstra [54], which observed that increased concentrations of limonene in dipalmitoyl phosphatidylcholine liposomes gradually lowered the melting peak temperature (T_m) and widened the peak.

In vitro release of TRF

Figure 4 compares the cumulative percentage of TRF released at different time intervals from the M5 sample and the control samples including Plain MCT 10% and Transcutol® 10%. At 0.5 hour, the descending order of TRF release was Plain MCT 10% followed by M5 and lastly Transcutol® 10%. The descending order then changed at 6 hour with M5 followed by Transcutol® 10 % and finally Plain MCT 10%. The optimized sample (M5) containing both D-limonene and squalene at 5% had an initial release of 7.72% and was continued to increase release for an additional 5.5 hour and finally achieved the highest drug release of 43.85% at 6 hour. This phenomenon could be attributed to the inverse relationship between TRF release and EE. EE is a metric that demonstrates the capacity of a formulation to retain the drug, and hence a higher EE theoretically indicates a delayed release rate [37]. Data from Table 2 were in good correlation with this observation, as M5 achieved the highest EE of 98.471% ± 0.116% among all the samples. The initial release from M5 was low and slow due to the encapsulation of TRF within the niosomal bilayers which acted as a strong barrier to drug release. The high EE entrapped a significant amount of TRF within the structure, thus preventing rapid diffusion and resulting in a slower initial release.

Table 3 summarizes the correlation coefficients (R^2) and the release exponent (n). Figure 5 shows plots of the release kinetics of TRF from the PNG formulations. The data of the M5 sample fitted best to Higuchi's diffusion model since it has the highest R^2 value of 0.9877 when compared to other models. Therefore, the release of TRF from M5 was based on the Higuchian matrix diffusion-controlled mechanism, in which the release of drug from this matrix possibly was influenced by diffusion of the matrix [11]. The release of TRF from M5 increased steadily over time due to controlled diffusion through the swollen niosomal bilayers, fitting well with the Higuchi diffusion model. This sustained release behavior was preferred as it minimized the need for frequent application and improved patient compliance by maintaining therapeutic drug levels over an extended period [31].

CONCLUSION

In conclusion, the study highlighted that the types and concentrations of enhancers loaded in PNG could be optimized to obtain the enhanced drug release effect of the drug encapsulated in the PNG formulations. The optimal PNG formulation was identified to be the combination of both 5% D-limonene and 5% squalene. All the PNGs with semisolid forms exhibited pseudoplastic flow behavior with high EE and antioxidant property of the TRF. The FTIR spectra and DSC thermogram confirmed the encapsulation of TRF into the PNGs and their thermal stability. Niosomes prepared from PNG M5 showed the greatest TRF release as compared to the control samples including plain without TRF, plain MCT 10% and Transcutol® 10% which acted as the positive control. While the study presents promising results for the topical delivery of TRF using terpene-loaded PNGs, it did not directly evaluate the anti-aging effects of TRF. Although TRF is widely recognized for its antioxidant potential, its specific impact on skin aging was not investigated. Therefore, future studies should explore this aspect through *in vitro* and *in vivo* models focused on anti-aging outcomes. Clinical trials in human subjects are also recommended to assess the safety, pharmacokinetics, and therapeutic efficacy of these formulations for potential dermatological or cosmeceutical applications.

ACKNOWLEDGMENTS

The authors would like to thank Kuala Lumpur Kepong Berhad (KLK Malaysia) for sponsoring the TRF for the research.

AUTHOR CONTRIBUTIONS

All authors made substantial contributions to conception and design, acquisition of data, or analysis and interpretation of data; took part in drafting the article or revising it critically for important intellectual content; agreed to submit to the current journal; gave final approval of the version to be published; and agree to be accountable for all aspects of the work. All the authors are eligible to be an author as per the International Committee of Medical Journal Editors (ICMJE) requirements/guidelines.

FINANCIAL SUPPORT

This work was supported by the Ministry of Higher Education through the Fundamental Research Grant Scheme (FRGS/1/2024/WAS04/TAYLOR/03/1).

CONFLICTS OF INTEREST

The authors report no financial or any other conflicts of interest in this work.

ETHICAL APPROVALS

This study does not involve experiments on animals or human subjects.

DATA AVAILABILITY

All data generated and analyzed are included in this research article.

PUBLISHER'S NOTE

All claims expressed in this article are solely those of the authors and do not necessarily represent those of the publisher, the editors and the reviewers. This journal remains neutral with regard to jurisdictional claims in published institutional affiliation.

USE OF ARTIFICIAL INTELLIGENCE (AI)-ASSISTED TECHNOLOGY

The authors declares that they have not used artificial intelligence (AI)-tools for writing and editing of the manuscript, and no images were manipulated using AI.

REFERENCES

1. Ghazali NI, Mohd Rais RZ, Makpol S, Chin KY, Yap WN, Goon JA. Effects of tocotrienol on aging skin: a systematic review. Front Pharmacol. 2022;13:1006198. doi: https://doi.org/10.3389/FPHAR.2022.1006198/BIBTEX
2. Luebberding S, Krueger N, Kerscher M. Skin physiology in men and women: *in vivo* evaluation of 300 people including TEWL, SC hydration, sebum content and skin surface pH. Int J Cosmet Sci. 2013;35:477–83. doi: https://doi.org/10.1111/ICS.12068
3. Pham J, Nayel A, Hoang C, Elbayoumi T. Enhanced effectiveness of tocotrienol-based nano-emulsified system for topical delivery against skin carcinomas. Drug Deliv. 2016;23:1514–24. doi: https://doi.org/10.3109/10717544.2014.966925
4. Chu CC, Hasan ZABA, Tan CP, Nyam KL. *In vitro* antiaging evaluation of sunscreen formulated from nanostructured lipid Carrier and tocotrienol-rich fraction. J Pharm Sci. 2021;110:3929–36. doi: https://doi.org/10.1016/J.XPHS.2021.08.020
5. Nair RS, Billa N, Leong CO, Morris AP. An evaluation of tocotrienol ethosomes for transdermal delivery using Strat-M® membrane and excised human skin. Pharm Dev Technol. 2021;26:243–51. doi: https://doi.org/10.1080/10837450.2020.1860087
6. Mittal S, Chaudhary A, Chaudhary A, Kumar A. Proniosomes: the effective and efficient drug-carrier system. Ther Deliv. 2020;11:125–37. doi: https://doi.org/10.4155/tde-2019-0065
7. Madan JR, Ghuge NP, Dua K. Formulation and evaluation of proniosomes containing lornoxicam. Drug Deliv Transl Res. 2016;6:511–8. doi: https://doi.org/10.1007/S13346-016-0296-9/METRICS
8. Vora B, Khopade AJ, Jain NK. Proniosome based transdermal delivery of levonorgestrel for effective contraception. J Contr Release 1998;54:149–65. doi: https://doi.org/10.1016/S0168-3659(97)00100-4
9. Ibrahim MMA, Sammour OA, Hammad MA, Megrab NA. *In vitro* evaluation of proniosomes as a drug carrier for flurbiprofen. AAPS PharmSciTech. 2008;9:782–90. doi: https://doi.org/10.1208/S12249-008-9114-0/METRICS
10. Ahmed MA, Abdelgawad WY, Gad MK, Mohamed MI. A novel approach for the treatment of oral ulcerative lesion using mucoadhesive proniosome gel. J Drug Deliv Sci Technol. 2021;63:102460. doi: https://doi.org/10.1016/j.jddst.2021.102460
11. Shah H, Nair AB, Shah J, Jacob S, Bharadia P, Haroun M. Proniosomal vesicles as an effective strategy to optimize naproxen transdermal delivery. J Drug Deliv Sci Technol. 2021;63:102479. doi: https://doi.org/10.1016/J.JDDST.2021.102479
12. Nemr AA, El-mahrouk GM, Badie HA. Development and evaluation of proniosomes to enhance the transdermal delivery of cilostazole and to ensure the safety of its application. Drug Dev Ind Pharm. 2021;47:403–15. doi: https://doi.org/10.1080/03639045.2021.1890111
13. Shah J, Nair AB, Shah H, Jacob S, Shehata TM, Aly Morsy M. Enhancement in antinociceptive and anti-inflammatory effects of tramadol by transdermal proniosome gel. Asian J Pharm Sci. 2020;15:786–96. doi: https://doi.org/10.1016/j.ajps.2019.05.001
14. Oliveira ALS, Valente D, Moreira HR, Pintado M, Costa P. Effect of squalane-based emulsion on polyphenols skin penetration: *ex vivo* skin study. Colloids Surf B Biointerfaces 2022;218:112779. doi: https://doi.org/10.1016/J.COLSURFB.2022.112779
15. Lasó E, Drasar PB, Khripach VA. Topical administration of terpenes encapsulated in nanostructured lipid-based systems. Molecules 2020;25:5758. doi: https://doi.org/10.3390/MOLECULES25235758
16. Dash DK, Panda DS, Pattnaik S, Vaiswade R, Gupta G. Enhancing transdermal drug delivery: formulation and evaluation of simvastatin-loaded invasomes in carbopol gel for improved permeability and prolonged release. Braz J Pharm Sci. 2025;61:e23976. doi: https://doi.org/10.1590/S2175-97902025E23976
17. Baiomy AM, Younis MK, Kharshoum RM, Alsalhi A, Zaki RM, Afzal O, *et al*. Optimized delivery of Enalapril Maleate via polymeric Invasomal in-situ gel for glaucoma treatment: *in vitro*, *in vivo*, and histological studies. J Drug Deliv Sci Technol. 2025;106:106685. doi: https://doi.org/10.1016/J.JDDST.2025.106685
18. Teaima MH, Eltabeeb MA, El-Nabarawi MA, Abdellatif MM. Utilization of propranolol hydrochloride mucoadhesive invasomes as a locally acting contraceptive: *in-vitro*, *ex-vivo*, and *in-vivo* evaluation. Drug Deliv. 2022;29:2549–60. doi: https://doi.org/10.1080/10717544.2022.2100514
19. Koyama Y, Bando H, Yamashita F, Takakura Y, Sezaki H, Hashida M. Comparative analysis of percutaneous absorption enhancement by D-Limonene and oleic acid based on a skin diffusion model. Pharm Res. 1994;11:377–83. doi: https://doi.org/10.1023/A:1018904802566
20. Chen J, Jiang QD, Chai YP, Zhang H, Peng P, Yang XX. Natural terpenes as penetration enhancers for transdermal drug delivery. Molecules 2016;21:1709. doi: https://doi.org/10.3390/MOLECULES21121709
21. Schafer N, Balwierz R, Biernat P, Ochędzan-Siodłak W, Lipok J. Natural Ingredients of transdermal drug delivery systems as permeation enhancers of active substances through the stratum corneum. Mol Pharm. 2023;20:3278. doi: https://doi.org/10.1021/ACS.MOLPHARMACEUT.3C00126
22. Sakdiset P, Arce FJ, See GL, Sawatdee S, Sae Yoon A. Preparation and characterization of lidocaine HCl-loaded proniosome gels with skin penetration enhancers. J Drug Deliv Sci Technol. 2023;86:104639. doi: https://doi.org/10.1016/j.jddst.2023.104639
23. Schlich M, Lai F, Pireddu R, Pini E, Ailuno G, Fadda AM, *et al*. Resveratrol proniosomes as a convenient nanoingredient for functional food. Food Chem. 2020;310:125950. doi: https://doi.org/10.1016/j.foodchem.2019.125950
24. Tareen FK, Shah KU, Ahmad N, Asim.ur.Rehman N, Shah SU, Ullah N. Proniosomes as a carrier system for transdermal delivery of clozapine. Drug Dev Ind Pharm. 2020;46:946–54. doi: https://doi.org/10.1080/03639045.2020.1764020
25. El-Enin ASMA, Khalifa MKA, Dawaba AM, Dawaba HM. Proniosomal gel-mediated topical delivery of fluconazole: development, *in vitro* characterization, and microbiological evaluation. J Adv Pharm Technol Res. 2019;10:20. doi: https://doi.org/10.4103/JAPTR.JAPTR_332_18
26. Gentili A, Caretti F. Analysis of vitamins by liquid chromatography. In: Fanali S, Haddad PR, Poole CF, Schoenmakers P, Lloyd D, editors. Liquid chromatography: applications. Amsterdam, Netherlands: Elsevier. 2013. pp. 477–517. doi: https://doi.org/10.1016/B978-0-12-415806-1.00018-8
27. Ong TS, Chu CC, Tan CP, Nyam KL. Preparation and evaluation pumpkin seed oil-based vitamin E cream formulations for topical

application. J Oleo Sci. 2020;69:297–306. doi: https://doi.org/10.5650/JOS.ESS19250
28. Liu J, Han Y, Chen J, Zhang Z, Miao S, Zheng B, *et al.* MCT/LCT mixed oil phase enhances the rheological property and freeze-thawing stability of emulsion. Foods 2022;11:712. doi: https://doi.org/10.3390/FOODS11050712
29. Ali H, El-Sayed K, Sylvester PW, Nazzal S. Molecular interaction and localization of tocotrienol-rich fraction (TRF) within the matrices of lipid nanoparticles: evidence studies by differential scanning calorimetry (DSC) and proton nuclear magnetic resonance spectroscopy (1H NMR). Colloids Surf B Biointerfaces 2010;77:286–97. doi: https://doi.org/10.1016/J.COLSURFB.2010.02.003
30. Chu CC, Hasan ZAA, Tan CP, Nyam KL. *In vitro* safety evaluation of sunscreen formulation from nanostructured lipid carriers using human cells and skin model. Toxicol *In Vitro* 2022;84:105431. doi: https://doi.org/10.1016/J.TIV.2022.105431
31. Shah H, Nair AB, Shah J, Bharadia P, Al-Dhubiab BE. Proniosomal gel for transdermal delivery of lornoxicam: optimization using factorial design and *in vivo* evaluation in rats. Daru 2019;27:59–70. doi: https://doi.org/10.1007/S40199-019-00242-X
32. Ortiz AC, Yañez O, Salas-Huenuleo E, Morales JO. Development of a nanostructured lipid carrier (NLC) by a low-energy method, comparison of release kinetics and molecular dynamics simulation. Pharmaceutics 2021;13:531. doi: https://doi.org/10.3390/PHARMACEUTICS13040531/S1
33. Akombaetwa N, Ilangala AB, Thom L, Memvanga PB, Witika BA, Buya AB. Current advances in lipid nanosystems intended for topical and transdermal drug delivery applications. Pharmaceutics 2023;15:656. doi: https://doi.org/10.3390/PHARMACEUTICS15020656
34. Spanova M, Zweytick D, Lohner K, Klug L, Leitner E, Hermetter A, *et al.* Influence of squalene on lipid particle/droplet and membrane organization in the yeast *Saccharomyces cerevisiae*. Biochim Biophys Acta 2012;1821:647. doi: https://doi.org/10.1016/J.BBALIP.2012.01.015
35. Chiu CS, Huang PH, Chan YJ, Li PH, Lu WC. D-limonene nanoemulsion as skin permeation enhancer for curcumin prepared by ultrasonic emulsification. J Agric Food Res. 2024;15:100932. doi: https://doi.org/10.1016/J.JAFR.2023.100932
36. Albash R, Al-Mahallawi AM, Hassan M, Alaa-Eldin AA. Development and optimization of terpene-enriched vesicles (terpesomes) for effective ocular delivery of fenticonazole nitrate: *in vitro* characterization and *in vivo* assessment. Int J Nanomed. 2021;16:609–21. doi: https://doi.org/10.2147/IJN.S274290
37. El-Laithy HM, Shoukry O, Mahran LG. Novel sugar esters proniosomes for transdermal delivery of vinpocetine: preclinical and clinical studies. Eur J Pharm Biopharm. 2011;77:43–55. doi: https://doi.org/10.1016/J.EJPB.2010.10.011
38. Manosroi A, Jantrawut P, Manosroi J. Anti-inflammatory activity of gel containing novel elastic niosomes entrapped with diclofenac diethylammonium. Int J Pharm. 2008;360:156–63. doi: https://doi.org/10.1016/J.IJPHARM.2008.04.033
39. Schreier H, Bouwstra J. Liposomes and niosomes as topical drug carriers: dermal and transdermal drug delivery. J Contr Release 1994;30:1–15. doi: https://doi.org/10.1016/0168-3659(94)90039-6
40. Lin H, Li Z, Sun Y, Zhang Y, Wang S, Zhang Q, *et al.* D-Limonene: promising and sustainable natural bioactive compound. Appl Sci. 2024;14:4605. doi: https://doi.org/10.3390/APP14114605
41. Haußß T, Dante S, Dencher NA, Haines TH. Squalane is in the midplane of the lipid bilayer: implications for its function as a proton permeability barrier. Biochim Biophys Acta - Bioenerg. 2002;1556:149–54. doi: https://doi.org/10.1016/S0005-2728(02)00346-8
42. Anandakumar P, Kamaraj S, Vanitha MK. D-Limonene: a multifunctional compound with potent therapeutic effects. J Food Biochem. 2021;45:e13566. doi: https://doi.org/10.1111/JFBC.13566
43. Huang ZR, Lin YK, Fang JY. Biological and pharmacological activities of squalene and related compounds: potential uses in cosmetic dermatology. Molecules 2009;14(1):540–554. doi: https://doi.org/10.3390/MOLECULES14010540
44. Zengin H, Baysal AH. Antibacterial and antioxidant activity of essential oil terpenes against pathogenic and spoilage-forming bacteria and cell structure-activity relationships evaluated by SEM microscopy. Molecules 2014;19:17773–98. doi: https://doi.org/10.3390/MOLECULES191117773
45. Baccouri B, Rajhi I, Baccouri B, Rajhi I. Potential antioxidant activity of terpenes. 2021. doi: https://doi.org/10.5772/INTECHOPEN.96638
46. Machado ND, Gutiérrez G, Matos M, Fernández MA. Preservation of the antioxidant capacity of resveratrol via encapsulation in niosomes. Foods 2021;10:988. doi: https://doi.org/10.3390/FOODS10050988
47. Rodriguez R, Redman R. Balancing the generation and elimination of reactive oxygen species. Proc Natl Acad Sci U S A. 2005;102:3175–6. doi: https://doi.org/10.1073/PNAS.0500367102/ASSET/C9623043-0653-4B48-8850-9A337CF067BB/ASSETS/GRAPHIC/ZPQ0110576760001.JPEG
48. Setiadi, Hidayah N. The effect of papain enzyme dosage on the modification of egg-yolk lecithin emulsifier product through enzymatic hydrolysis reaction. Int J Technol. 2018;9:380–9. doi: https://doi.org/10.14716/IJTECH.V9I2.1073
49. Gorman M. The evidence from infrared spectroscopy for hydrogen bonding: a case history of the correlation and interpretation of data. J Chem Educ. 1957;34:304–6. doi: https://doi.org/10.1021/ED034P304
50. Xu Q, Wu Y, Saito H, Ofuchi Y, Setoyama H, Furuishi T, *et al*. Promoting activity of terpenes on skin permeation of famotidine. Chem Pharm Bull (Tokyo). 2023;71:111–9. doi: https://doi.org/10.1248/CPB.C22-00568
51. Shruthi PA, Pushpadass HA, Franklin MEE, Battula SN, Laxmana Naik N. Resveratrol-loaded proniosomes: formulation, characterization and fortification. LWT. 2020;134. doi: https://doi.org/10.1016/j.lwt.2020.110127
52. Savic SM, Cekic ND, Savic SR, Ilic TM, Savic SD. "All-natural" anti-wrinkle emulsion serum with Acmella oleracea extract: a design of experiments (DoE) formulation approach, rheology and *in vivo* skin performance/efficacy evaluation. Int J Cosmet Sci. 2021;43:530–46. doi: https://doi.org/10.1111/ICS.12726
53. El Maghraby GM, Ahmed AA, Osman MA. Penetration enhancers in proniosomes as a new strategy for enhanced transdermal drug delivery. Saudi Pharm J. 2015;23:67–74. doi: https://doi.org/10.1016/J.JSPS.2014.05.001
54. El Maghraby GMM, Williams AC, Barry BW. Interactions of surfactants (edge activators) and skin penetration enhancers with liposomes. Int J Pharm. 2004;276:143–61. doi: https://doi.org/10.1016/J.IJPHARM.2004.02.024
55. Cekic ND, Savic SM, Savic SD. Dynamic-mechanical thermoanalysis test: a rapid alternative for accelerated freeze-thaw stability evaluation of W/O emulsions. Drug Dev Ind Pharm. 2019;45:1896–906. doi: https://doi.org/10.1080/03639045.2019.1672718
56. Mezger T. The rheology handbook - for users of rotational and oscillatory rheometers. Appl Rheol. 2002;12:232. doi: https://doi.org/10.1515/ARH-2002-0029
57. Pippa N, Pispas S, Demetzos C. The metastable phases as modulators of biophysical behavior of liposomal membranes: the role of biomolecular sculpture of polymeric guest. J Therm Anal Calorim. 2015;120:937–45. doi: https://doi.org/10.1007/S10973-014-4116-5

How to cite this article:
Fong TT, Chaiku P, Nyam KL, Chu CC. Development and evaluation of a proniosomal gel for palm tocotrienol-rich fraction topical delivery. J Appl Pharm Sci. 2025;15(12):046-059. DOI: 10.7324/JAPS.2025.v15.i12.6